PIV characterization of a separated flow controlled by a DBD actuator

IOP Conf. Series: Journal of Physics: Conf. Series **1249** (2019) 012012 doi:10.1088/1742-6596/1249/1/012012

PIV characterization of a separated flow controlled by a DBD actuator

G. Zoppini, L. Di Vinci, G. Campanardi, A. Zanotti and M. Belan

Politecnico di Milano, Dipartimento di Scienze e Tecnologie Aerospaziali, Via La Masa 34, 20156 Milano, Italy

E-mail: giulia.zoppini@mail.polimi.it

Abstract. This work investigates the three-dimensional effects of a dielectric barrier discharge actuator as a stall recovery device. The actuator is installed on a NACA0015 airfoil with a 930 mm span and a 300 mm chord and the exposed electrode has periodic triangular tips specifically designed for the case under study. It was tested at progressively increasing velocities, up to 35 m/s corresponding to a Reynolds number of 7×10^5. The PIV technique has been used to characterize the flow morphology along the model span, identifying the flow region mainly sensitive to the plasma effect and suggesting possible design improvements to achieve a better efficiency.

1. Introduction

The research on plasma actuators developed quite rapidly in the last decades thanks to their interesting performances. In particular, in the recent years a constantly increasing interest was demonstrated towards the application of DBD (*dielectric barrier discharge*) actuators to flow control [1, 2]. Their classical structure consist of two electrodes separated by a dielectric layer. Powered by an external source, that applies an alternating voltage between the electrodes, they induce a ionic wind capable of accelarating the flow in the proximity of the wall they are mounted on. Detailed descriptions of their working principles can be found in [2, 3, 4]. These devices rapidly spread thanks to their capability to directly convert electric into kinetic energy without involving moving mechanical parts. This makes them light and easy to mount and substitute, appealing characteristics in the aeronautical field. Besides, they have a very short response time which allows real-time control applications also at high frequency. Yet, their efficiency in energy conversion can still be improved.

Plasma actuators, especially DBD, have already been used to control flows with Reynolds numbers above 10^6. When aligned with the freestream, they can work as vortex generators, with the advantage that they can be operated only when needed. If applied to control stall on airfoils, they are often installed closed to the leading edge, upstream of the expected separation point [5]. In this way, they successfully manipulated separated flows [6], boundary layer laminar-to-turbulent transitions [7], and shear layers [8]. Burst modulation of the voltage signal improves the control performances in particular for a deep stall configuration [5], provided that the frequency and the duty cycle are suitably chosen [9]. Recently, also nano-second pulsed DBDs demonstrated highly effective in manipulating separation for Reynolds numbers even above

2×10^6, [10]. When located near the trailing edge, actuators can act as a flap, increasing the lift coefficient [5, 11].

In order to optimize a DBD, it is possible to act either on the input signal, [2, 12], or on the geometry of the exposed electrode, that should always be designed for the particular application [13]. Sharp tips increase ionic wind and thrust [12], and they induce also transverse velocity components that originate streamwise vortex structures. In turn, these vortices improve the boundary layer mixing and the control capabilities of the device. In this study, the multi-tip geometry explored in [14] is applied, choosing an exposed electrode with triangular tips separated by suitable spacings.

A wide branch of the research on plasma actuators is dedicated to their application to airfoils or uses the airfoils as test cases. The major part of these works, though, only characterize the actuator-flow interaction in correspondence of the central sections, focusing on a two-dimensional analysis. Only few studies, such as [5, 10], introduce purposely designed devices, as wide end-plates, to counteract the three-dimensional structures development. Instead, in the present study an opposite approach is followed: the model airfoil is not even provided with end-plates in order to allow the intrinsic complete development of the three-dimensional structures typical of the flow field aerodynamics. This is actually the core investigation of this work, during which the PIV measurements were repeated on five spanwise distributed tips in order to analyse the flow modifications. In this way, the flow region most sensitive to the plasma effect is identified, suggesting possible design improvements to achieve a better efficiency.

This work presents at first the experimental set-up, followed by its validation through PIV measures performed on the central sections. Afterwards, the spanwise distributed sections are progressively characterized, showing the influence of the actuator on the three-dimensional flow. Finally, some considerations on the device efficiency are reported.

2. Experimental Set-up

The principal element of the set-up is the NACA0015 model built for this experiment. Made of UREOL, a polyurethane foam extremely rigid and electrically insulating, it has a span $S = 930$mm and a chord $c = 300$mm. The span was constrained by the test chamber width, and no end-plates were integrated to allow the natural development of the three-dimensional flow, which is not negligible even if the airfoil model has a relatively good aspect ratio S/c =3.1.

To couple the model with the pre-existing supporting structure, two matching side ribs and tubular shafts were built. Since the high voltage cable was clamped on them during the tests, to improve the insulation the left hand side components are made of Nylon. The right hand ones instead are made of aluminium alloy, to improve the pitching constraint. They allow an easy modification of the pitch angle firmly holding the airfoil during the tests. The actuator electrodes are applied on a *C-shaped* plexiglass insert that is then mounted on the leading edge of the profile. In Figure 1 the complete assembly is shown.

To perform the PIV measures, the model was mounted in the "Sergio De Ponte" wind tunnel, a closed circuit system with a test section of $1 \times 1.5 \times 3$m. For the airfoil described above, the resulting wind tunnel blockage is negligible even at high angles of attack. Two PIV cameras with $2Mpx$ *CCD* sensors were needed to capture the whole upper flow field. Both rigidly constrained to the support structure, the front camera was fitted with a 50mm lens, and the rear one with a 24mm. This allowed to have an higher definition on the correspondence of leading edge and a wider flow field on the mid-rear section. The laser system produces 200mJ impulses of 532nm wavelength. It was synchronized with the cameras to correctly capture the flow images. *Di-Ethyl-Hexyl-Sebacat* (DEHS) was used as seeding fluid.

The geometrical optimization of the exposed electrode was the most challenging part of the set-up phase. The first design choice was the use of triangular tips on the electrode, that can induce a higher ionic wind and inject a larger momentum in the streamwise direction [12, 14, 15].

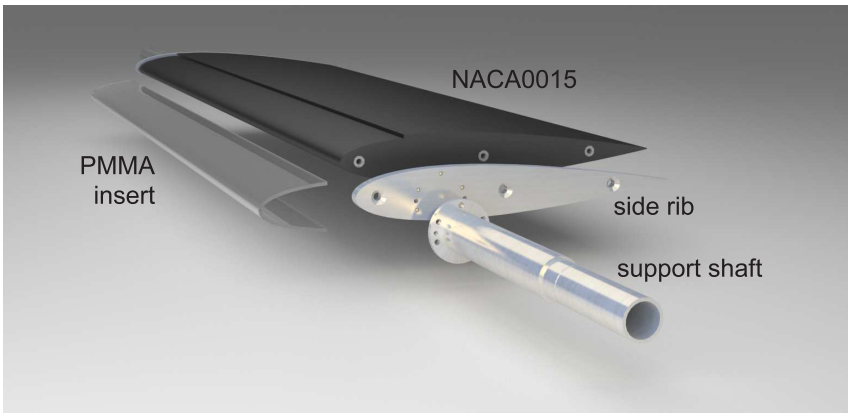

Figure 1. NACA0015 assembly

For a triangular tip, the sharpness corresponds to the length-to-base ratio $r = h/w$: values of r above the unity have proven to create high electric fields and induced velocities, and can reach 4 or 5 still preventing excessive damages due to heat or arcs formation. Accordingly, in this work the tips have sharpness $r = 5$. The *tip effect* on lift enhancement and stall control is expected to scale as $1/U_\infty^2$ [15, 19], so as the freestream velocity grows it loses intensity. However, literature demonstrated that optimizing the tips spacing a better authority can be kept at higher velocities. In fact, with this geometry the actuator works also as a vortex generator (VG), as described in [14, 19]. The induced velocity is always orthogonal to the electrode perimeter, so that between a tips pair it gives rise to two counter rotating vortex structures, improving the mixing of the boundary layer, as shown in Figure 2. If the tip spacing d is appropriately chosen, this effect can significantly enhance the actuator authority.

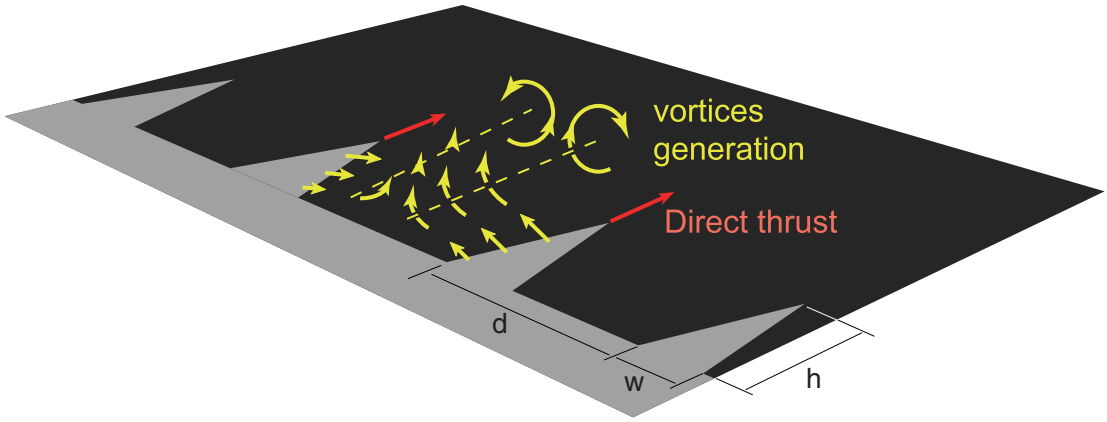

Figure 2. Simplified plane sketch of the DBD effects and main geometrical parameters.

The optimal inter-tip spacing has been found to be related with the discharge length measured at working voltage [17], and turns out to be twice this length. Actually this scaling rule is based on the assumption that the optimal spacing only depends on the discharge properties and not on the incoming boundary layer thickness. Under this hypothesis, bench tests were conducted, following the method described in [18], to define the spacing for this set-up. The available power supply can provide 40kV_{pp}, leading to a discharge length of 18 mm, thus the tip spacing was set to $d = 36\text{mm}$.

After defining the tip sharpness r and the spacing d, the tip length h requires a more delicate analysis, striclty linked to U_∞. In literature, the formation and evolution of the streamwise vorticity ω_x was studied at first for low freestream values [16], then its characterization was extended to higher velocities in [17]. For the present actuator, starting from a dimensional analysis of the x-component of the vorticity transport equation, the VG effect appears as a reorientation of the spanwise vorticity ω_z carried by the approaching boundary layer. This process originates the ω_x component, but to correctly occur, fluid particles have to lay over the actuator for a certain time. The main time scale is the convective one, $T_C = h/U_\infty$ where h is the tip length; instead the viscous time $T_\nu = \delta^2/\nu$ where δ is the boundary layer thickness turns out to be much longer ($T_\nu \gg T_C$), so that an inviscid analysis is sufficient. To quantify the reorientation time scale, we should recall that the vortex structures lay within the boundary layer (and their scale is exaggerated for clarity in Figure 2). This means that a fluid particle travelling in the external flow over a tip is dragged down toward the wall while it undergoes a rotation around the streamwise direction. For the transverse motion, a velocity in the order of the ionic wind V_i can be associated to this phenomenon, and it can be considered that the particle has to sweep almost half the inter-tip spacing. So the circulation time scale can be estimated as $T_R = d/2V_i$. In order to allow a complete and correct reorientation of the vorticity, the primary constraint becomes $T_C \geq T_R$, or at least T_C and T_R in the same order of magnitude.

Assuming a freestream velocity U_∞ in the order of 20m/s (Re=400k), and accounting for the time scales above defined the tips length h can be set to 50mm, a value compatible with the model size. However, during the test campaign the actuator was tested also at higher freestream velocities demonstrating significant control capabilities up to U_∞=35m/s. Starting from these results, the spanwise measurements were performed at an intermediate velocity, namely U_∞=30m/s, where the $T_C \geq T_R$ constraint is only approximately satisfied but the test conditions correspond to Re=600k, a value closer to the ones of interest in real applications.

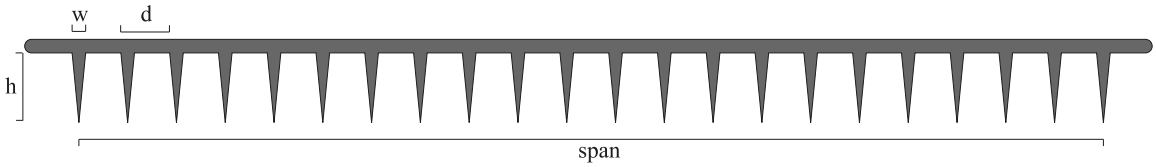

Figure 3. Exposed electrode geometry

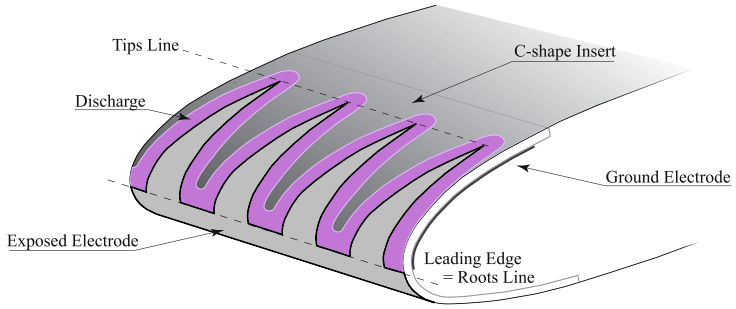

Figure 4. Particular of the DBD assembled on the airfoil

In conclusion, the final design is based on tips of sharpness $r = 5$, length h=50mm (this sets also the tip width w = 10mm) and spacing d=36mm, so that the device has 20 tips with an overall span between tips of 756mm. The exposed electrode geometry is shown in flat form in Figure 3. This electrode was mounted on the external surface of the C-Shaped PMMA insert

as shown in Figure 4, whereas a rectangular ground electrode with dimensions of 800 × 60mm was applied on the inner surface. They are both manufactured from a 125μm thick aluminium foil. The assembled model was then mounted in the test chamber to begin the experimental campaign.

3. Results

This section presents the results of the PIV analysis, starting from the study of the central sections at the design velocity of 20m/s. This configuration allowed to perform a validation of the set-up and a first test of the actuator. Afterwards, the airspeed was increased to the higher value of 30m/s and the different spanwise sections were analysed, to study the actuator effect over the whole wing. A sketch of the actuator and the PIV measurement planes is reported in Figure 5. In what follows, the term *root* identifies the middle point of the inter-tip distance (18mm from each tip), as indicated by the yellow line corresponding to section R in Figure 5.

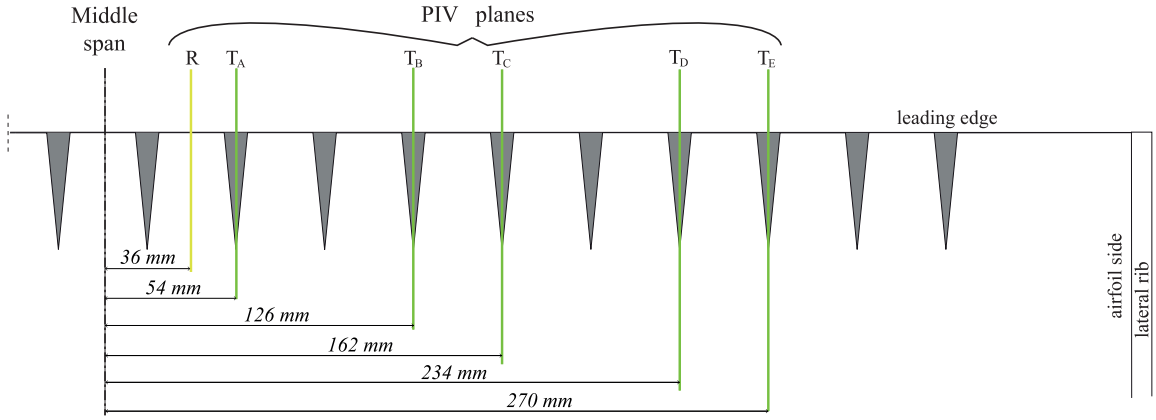

Figure 5. PIV measurement planes: alignment with the actuator on the airfoil surface

3.1. Central Sections analysis at 20m/s

As usual in literature, the first measures were performed on the mid-span region, starting from the T_A plane. It was initially analysed at the design velocity of 20m/s under early stall conditions, with an angle of attack $\alpha = 14.5°$. The actuator supply was a steady sinusoid with frequency 650Hz.

In the plasma off flow field, Figure 6, the separation point lays at about 30% of the chord, and the recirculation bubble extends up to the trailing edge. With plasma on, Figure 7, the separation point is shifted downstream, and the recirculation bubble is significantly reduced: they are confined within the quarter of chord from the trailing edge. The streamlines acceleration is well visible, in fact they are deflected toward the profile. These modifications bring beneficial effects on the local pressure and lift coefficients C_P, C_L.

Both the effects of momentum injection and vortex generation influence the flow around the airfoil. As shown in Figure 2, the direct momentum injection is mainly due to the tips because of their high local electric field, whereas the inter-tip spacing is characterized by the vortical motion. This induces different modifications on the local flow field, evidenced in what follows by comparing the measures performed at the tip and root planes T_A and R.

Figure 8 shows that the plasma off flow field at the root is similar to the one at the tip. This indicates that the passive effect of the actuator at this Reynolds number and beyond is weak and can be neglected. Considering the plasma on configuration, Figure 9, it is observed that both the shift in the separation point and the streamlines acceleration are milder. This difference may

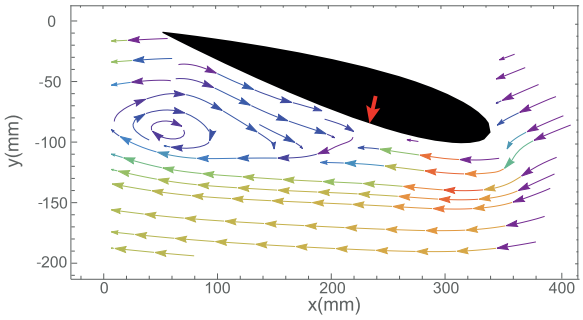

Figure 6. Plasma off flow field at T_A for $\alpha = 14.5°$ and U_∞=20m/s

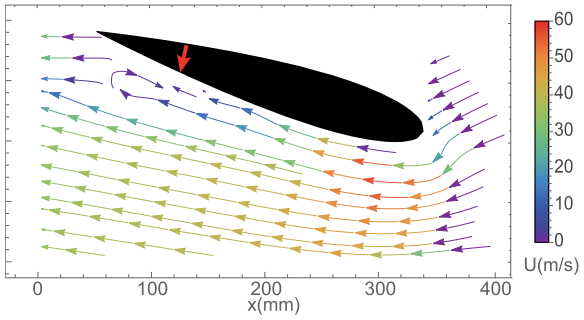

Figure 7. Plasma on flow field at T_A for $\alpha = 14.5°$ and U_∞=20m/s

be explained by recalling that on the root plane the ionic wind has a component normal to the surface with outgoing direction (Figure 2), whereas the tips induce a nearly parallel wind on a further chordwise position with respect to the roots. Therefore, the reduction of the recirculation bubble is significant on both the planes under study, but the local flow pattern generated by the actuator partially retains the shape of the active electrode.

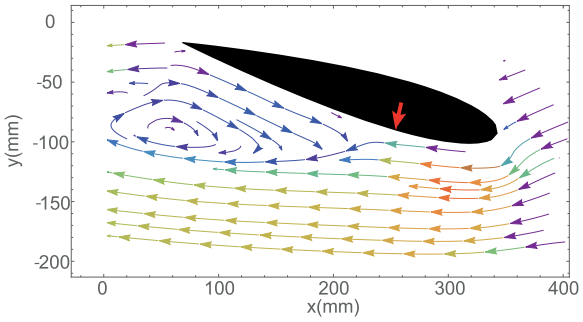

Figure 8. Plasma off flow field at R for $\alpha = 14.5°$ and U_∞=20m/s

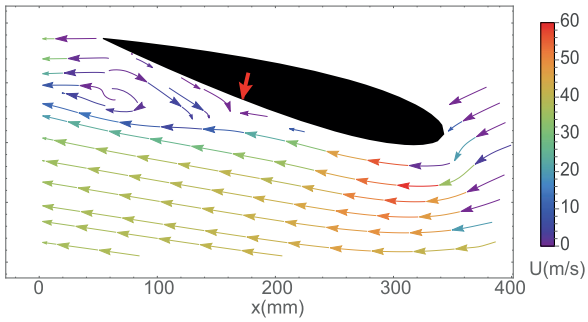

Figure 9. Plasma on flow field at R for $\alpha = 14.5°$ and U_∞=20m/s

To test the actuator under more severe conditions, a deep stall configuration with $\alpha = 22°$ was introduced. Some researches [6, 20] underlined that an effective control requires a direct interaction with the vortex structure formation and detachment. Therefore, a pulsed supply mode with a modulating frequency f_m close to the vortex shedding one is usually applied. The reduced frequency, defined as $F^+ = f_m\ c/U_\infty$ in [9], is often used to characterize the modulation and the most effective value for stall control is widely recognized to be close to the unity. Also in the present case, F^+ was set to 1 while keeping the carrier frequency at 650Hz as above. Another useful parameter is the duty cycle, varied from 20% to 50% during the tests. Within this range, it does not significantly modify the effect of the actuator on the flow, but lower values automatically give lower power consumptions.

Figure 10 shows the plasma off flow field. The separation point lays at about 2% of the chord, and the recirculation bubble is much larger than for early stall, expanding also outside the captured region. The actuator is not expected to reattach the flow, but in Figure 11, representing the plasma on configuration, a major change in the shape and size of the recirculation bubble and a mild shift in the separation point are observed. Owing to the pulsed actuation, the bubble center is shifted toward the profile and the recirculating structure is now well visible.

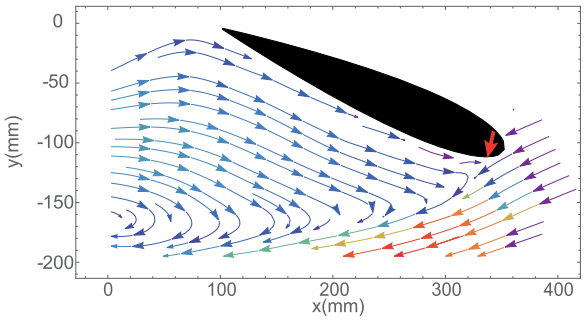

Figure 10. Plasma off flow field at T_A for $\alpha = 22°$ and U_∞=20m/s

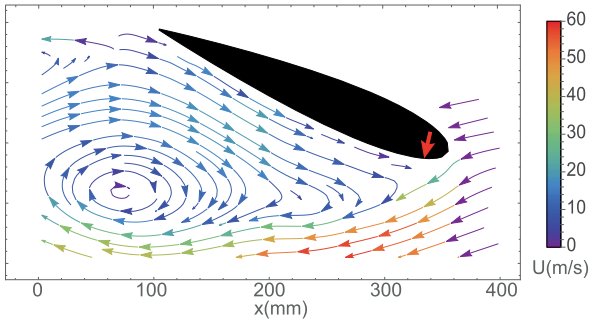

Figure 11. Plasma on flow field at T_A for $\alpha = 22°$ and U_∞=20m/s

Further tests were performed to define the maximum operational velocity at which the device affects the flow, that turned out to be in the 35 to 40 m/s range. Figures 12, 13 show the flow fields for U_∞ = 35 m/s at α = 14.5°. There are still a slight shift of the separation point and a small reduction of the recirculation bubble. The flow modifications are better visible by analysing the cross-wake velocity, reported in Figure 14, where the actuator effect appears to be a wake width reduction.

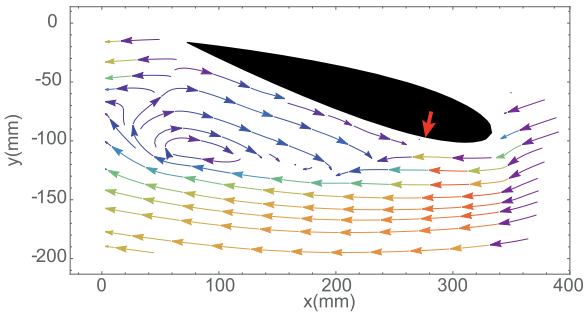

Figure 12. Plasma off flow field at T_A for $\alpha = 14.5°$ and U_∞=35m/s

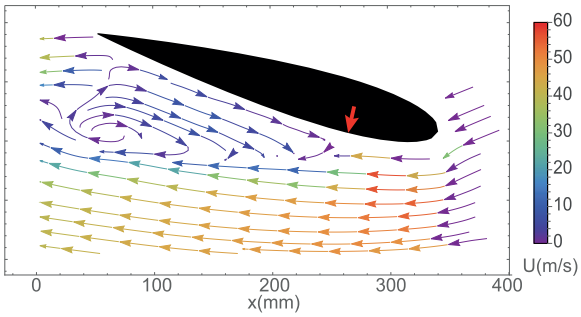

Figure 13. Plasma on flow field at T_A for $\alpha = 14.5°$ and U_∞=35m/s

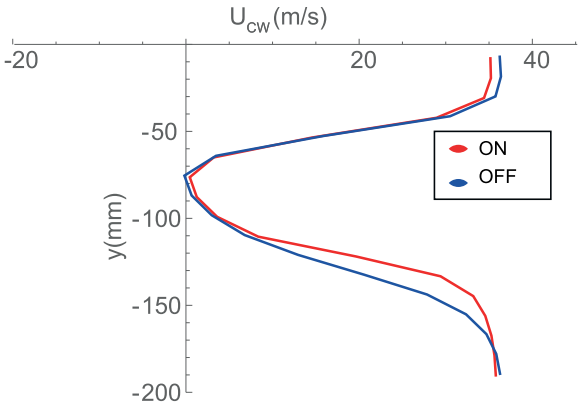

Figure 14. Cross wake velocity at T_A for $\alpha = 14.5°$ and U_∞=35m/s

As expected, outside the recirculation region the velocity is close to the U_∞ value. Although, it is noted that in the proximity of the airfoil the plasma on curve, in red, shows a lower speed than the plasma off one, in blue. An explanation may be that the actuator is actually supposed to modify the flow field around the whole airfoil, influencing also the circulation and the stagnation point location on the pressure side. This would lead to a further enhancement of the lift coefficient, even if the captured flow field is too narrow to confirm this hypothesis.

The next section is specifically devoted to the flow characterization along the span, performed at U_∞= 30m/s as explained in §2.

3.2. Spanwise sections analysis at 30m/s, $\alpha = 14.5°$

In this section, the effect of the actuator on the spanwise tips T_A, T_B, T_C, T_D, T_E at U_∞=30m/s and $\alpha = 14.5°$ is analysed. All the images collected for the lateral planes were corrected for the perspective effect: since the cameras are fixed, they capture wider flow fields for the outer sections than for the central ones, requiring a rescaling.

Beginning with the analysis of T_A, it is observed that in the plasma off configuration, Figure 15, the flow field is similar to the one at 20m/s: the separation point lays at about 20% of the chord and the recirculation bubble extends up to the trailing edge. In the plasma on case, Figure 16, the actuator still demonstrates a strong authority despite the velocity increase. It shifts the separation point of about 20mm and reduces the recirculation bubble extension, displacing its center toward the profile. Also the acceleration and deflection of the streamlines is evident, and should lead to an increase of the overall pressure and lift coefficients.

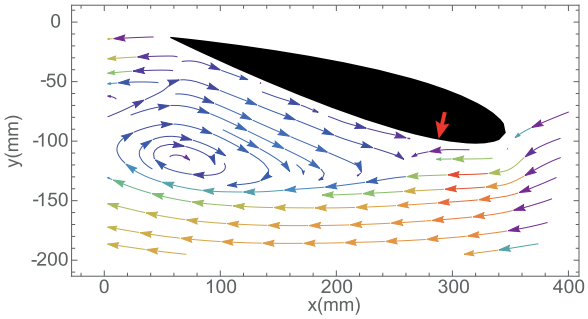

Figure 15. Plasma off flow field at T_A for $\alpha = 14.5°$ and U_∞=30m/s

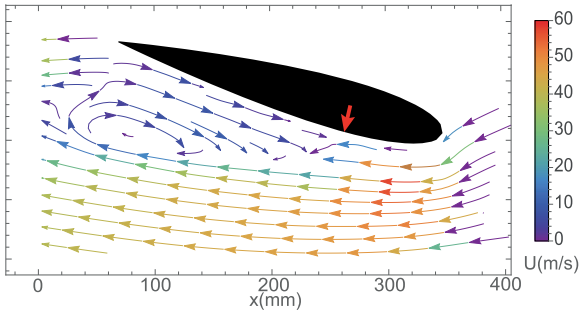

Figure 16. Plasma on flow field at T_A for $\alpha = 14.5°$ and U_∞=30m/s

Moving along the span, Figure 17 shows T_B in the plasma off condition. Due to the classical flow geometry over a finite wing, the separation point is naturally shifted toward the trailing edge. Under the actuator effect, Figure 18, it is further moved of about 25mm, and a visible reduction of the recirculation bubble is achieved. At the same time, the external streamlines are displaced and realigned with the airfoil profile. Then, the actuator still has strong authority on the flow and on the local forces, even if the three-dimensional separation pushes the natural detachment point downstream with respect to the actuator tip position.

At T_C the flow field is still similar, but the separation point and the recirculation bubble in the plasma off configuration lay within 25% of chord from the trailing edge, as shown in Figure 19. With plasma on, Figure 20, they are pushed further downstream of about 20mm, influencing a narrower region of the airflow. The external streamlines are again accelerated and deflected toward the profile. Thus the actuator seems to influence the lift coefficient also in correspondence of this section.

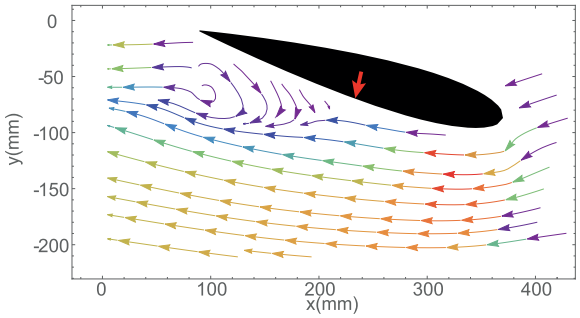

Figure 17. Plasma off flow field at T_B for $\alpha = 14.5°$ and U_∞=30m/s

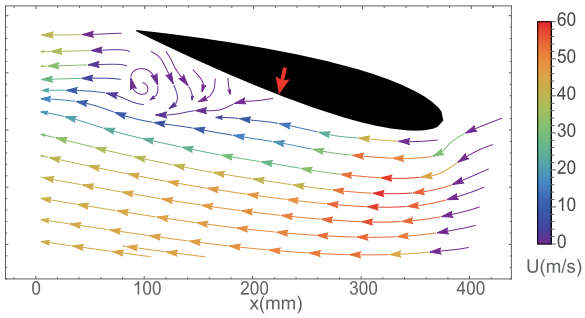

Figure 18. Plasma on flow field at T_B for $\alpha = 14.5°$ and U_∞=30m/s

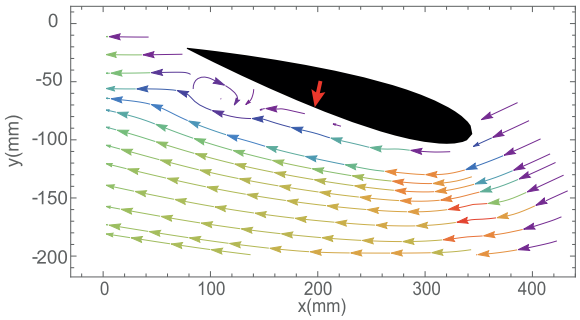

Figure 19. Plasma off flow field at T_C for $\alpha = 14.5°$ and U_∞=30m/s

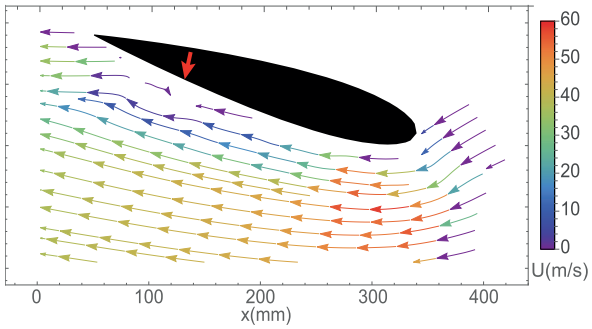

Figure 20. Plasma on flow field at T_C for $\alpha = 14.5°$ and U_∞=30m/s

Finally T_D and T_E are studied: here in the plasma off configuration, Figures 21, 23, the flow is not separated. The effect of the actuator is still visible from the slight changes in the streamlines in Figures 22 and 24; however the local flow remains substantially attached independently of the actuator effect, and this indicates that an electrode of lower span could have very similar flow control capabilities with a lower power consumption.

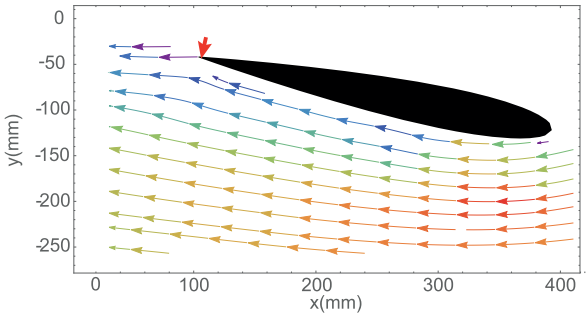

Figure 21. Plasma off flow field at T_D for $\alpha = 14.5°$ and U_∞=30m/s

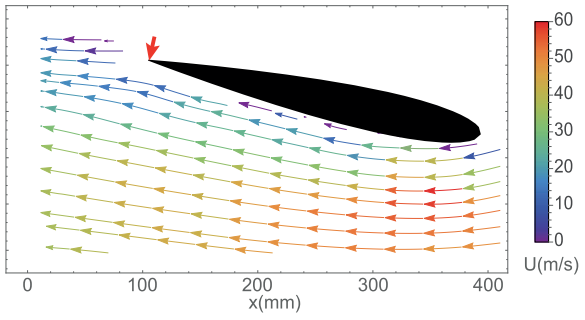

Figure 22. Plasma on flow field at T_D for $\alpha = 14.5°$ and U_∞=30m/s

Collecting the data from the different PIV planes, an overall representation of the 3D separation line over the airfoil surface can be obtained, as in Figure 25, both for plasma off and on configurations. It is worth to note that a refined scan with many more PIV planes would lead to a similar shape, with a superimposed undulation due to the tip–root variations described

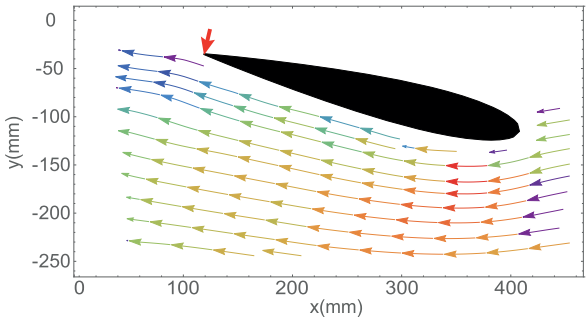

Figure 23. Plasma off flow field at T_E for $\alpha = 14.5°$ and U_∞=30m/s

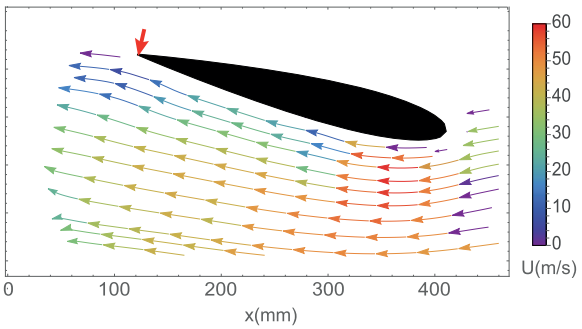

Figure 24. Plasma on flow field at T_E for $\alpha = 14.5°$ and U_∞=30m/s

in §3.1. The plasma off separation line, in blue, shows the typical contour for a finite wing, that is known to appear even in a wind tunnel test when, as in this case, large end plates are not purposely introduced. In the plasma on case, in red, the separation line is shifted backward. This displacement may seem mild, but involves an important area where the pressure changes on the model surface can produce significant lift variations. As evidenced above, even in this figure it can be observed that in the lateral sections the separation points for plasma on and off are very closed to each other or coincide, suggesting that a similar performance could be achieved by removing the outer tips of the actuator.

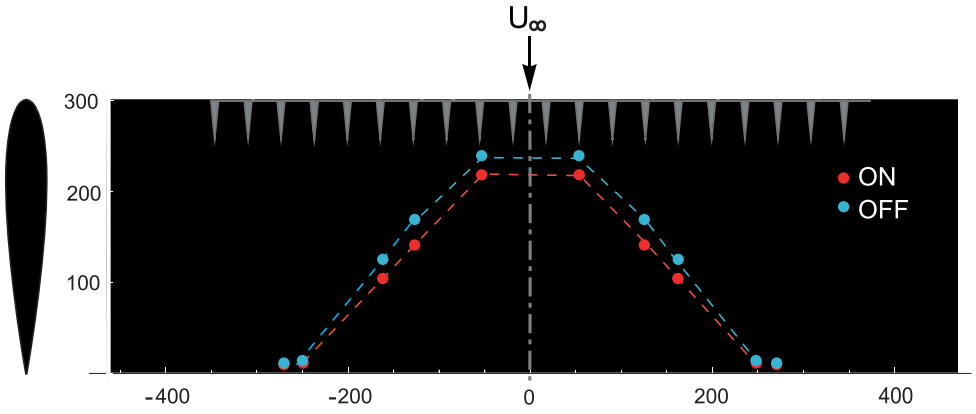

Figure 25. Complete separation line at $\alpha = 14.5°$, U_∞=30m/s

3.3. Spanwise sections analysis at 30m/s, $\alpha = 22°$

The same spanwise analysis has been performed in deep stall configuration. In this case the actuator is operated in pulsed mode with modulation $F^+ = 1$, and duty cycles between 20 and 50%, as previously described. The same spanwise tips T_A, T_B, T_C, T_D, T_E are studied, comparing their flow fields. Again the analysis can start from T_A, whose plasma off condition is reported in Figure 26. Similarly to the 20m/s case, the separation point is close to the leading edge of the airfoil, and the recirculation bubble is widely extended. Despite the higher velocity, in the plasma on configuration, Figure 27, the separation point is slightly shifted downstream, and the bubble is significantly reduced and pushed closer to the profile, presumably leading to a useful drag reduction.

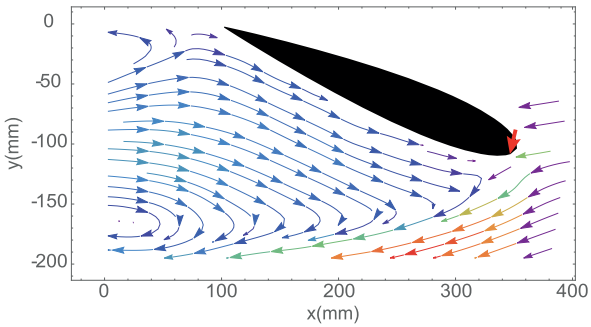

Figure 26. Plasma off flow field at T_A for $\alpha = 22°$ and U_∞=30m/s

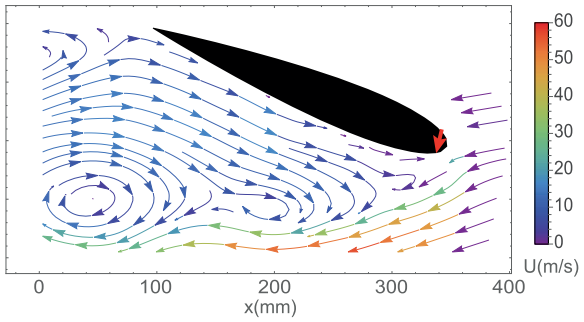

Figure 27. Plasma on flow field at T_A for $\alpha = 22°$ and U_∞=30m/s

In Figure 27 the flow pattern in the recirculating region includes two substructures, that can be easily explained as effects of the pulsed actuation; however, since these velocity fields are obtained as averages, this indicates also an insufficient convergence of the averaging process on this particular case. Apart from this exceptional field, the deep stall results at 20m/s and the other spanwise planes at 30m/s converge regularly, confirming the significant effect of the actuator on the flow.

Figure 28 represents the flow field at T_B in the plasma off condition. It is noted that moving toward external sections the separated field naturally decreases, even if it still begins in the proximity of the leading edge. With plasma on, Figure 29, a wake reduction effect is again visible and leads to a decrease in the momentum drop that presumably brings a better drag coefficient.

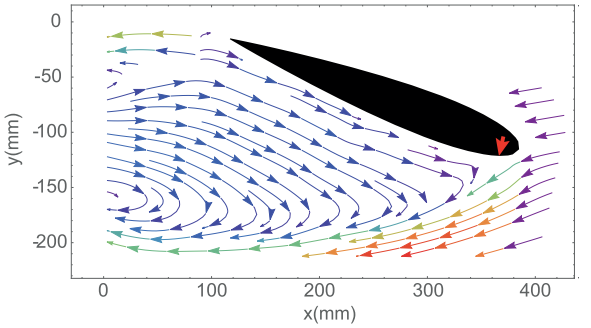

Figure 28. Plasma off flow field at T_B for $\alpha = 22°$ and U_∞=30m/s

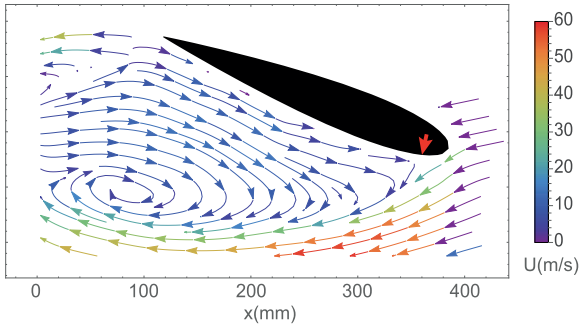

Figure 29. Plasma on flow field at T_B for $\alpha = 22°$ and U_∞=30m/s

Similarly, on the outer sections, the separation point is shifted backward, and the recirculation region is further reduced both naturally and through the actuator effect, leading to a lower loss in momentum and a faster recovery, as shown in Figures 30, 31, 32, 33.

3.4. Actuator effectiveness

In section §3.2, it was shown that the separated region sensitive to the actuator lies in the central part of the model, whereas the lateral regions are only marginally influenced. Therefore, an actuator of shorter span could presumably give similar effects with less electric power and more efficiency. To determine the capabilities of the device in a realistic application, an estimation of its effectiveness is needed. For given U_∞ and α conditions, a useful quantity is the effectiveness

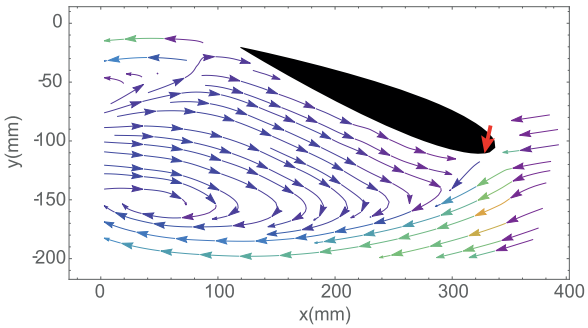

Figure 30. Plasma off flow field at T_C for $\alpha = 22°$ and U_∞=30m/s

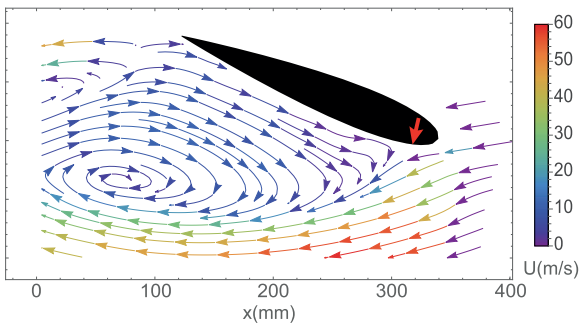

Figure 31. Plasma on flow field at T_C for $\alpha = 22°$ and U_∞=30m/s

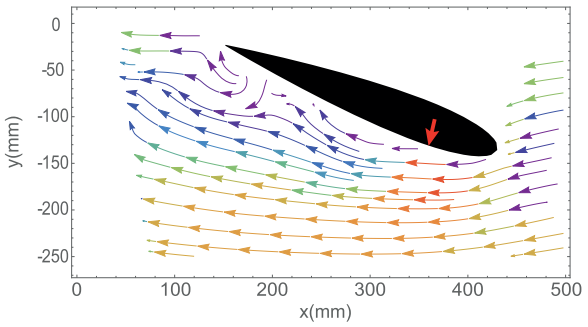

Figure 32. Plasma off flow field at T_E for $\alpha = 22°$ and U_∞=30m/s

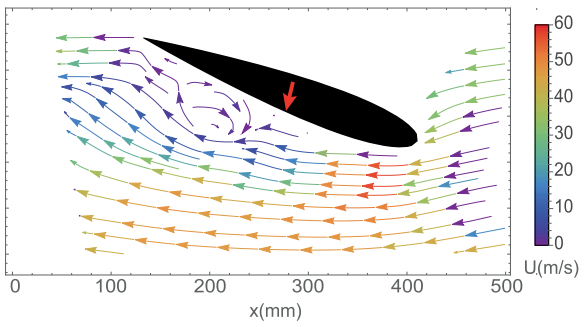

Figure 33. Plasma on flow field at T_E for $\alpha = 22°$ and U_∞=30m/s

$\varepsilon = \Delta L/W_0$ in N/W, where ΔL is the lift increase achieved through the actuator, and W_0 is the power it requires. The value of ΔL can be obtained from *PIV* data elaboration when the whole field of motion around the airfoil is known, or by direct measurements of aerodynamic forces, not available in this study. However, by modifying the actuator length the *relative* changes of effectiveness can be estimated as follows.

Some bench tests were performed to evaluate the power consumption at the operating conditions: with a steady sinusoidal wave of amplitude 40kV$_{pp}$ at the standard frequency of 650Hz, the actuator requires a power $W_0 = 169.0$W. The results analysis suggests to remove the lateral parts of the actuator, and recalling that the passive effects of the unpowered electrode are weak, the flow field over the whole model will remain approximately the same with a shorter DBD. In turn, powering the reduced actuator should give the same overall ΔL with a reduced power consumption. The power varies linearly with the tips number and the total span of the actuator, and the original exposed electrode has 20 tips, so without the 8 external ones, four on each side, the original power $W_0 = 169$W should decrease to $W_1 = 101.4$W, leading to an effectiveness growth $\varepsilon_1/\varepsilon_0$ about 60%. Even a more prudential modification, removing only 6 of the outer tips, would lead to a power $W_2 = 118.3$W and to an interesting effectiveness growth $\varepsilon_2/\varepsilon_0$ about 40%.

4. Conclusions

This work characterizes the effect of a DBD actuator over an airfoil, considered as a three-dimensional body. In particular through PIV measurements, five spanwise distributed sections were studied under early and deep stall conditions. The actuator-flow interaction takes place along the span, and the complete 3D separation line is displaced toward the trailing edge when

the DBD is activated. The local effects are in general a reduction of the recirculating region size and a shift in the separation point, unless the flow is already attached. In fact, in correspondence of the external sections the flow is always naturally attached and the actuator creates only slight modifications of the local streamlines. This point suggests that a similar separation control could be achieved by an actuator of shorter span, with a corresponding lower power consumption: under the assumption that the actuator effect is kept unaltered, the effectiveness measured in terms of N/W can increase in this way up to 60%.

Two main conclusions can be drawn from the above results. In experiments on airfoils, the deduction of 2D properties is reliable only when effective devices as end/splitter plates are installed to counteract the undesired 3D structure of the flow. In experiments on real wings and 3D bodies, a suitable scan of the flow field is a good diagnostic to identify the region most sensitive to a flow control technique.

References

[1] Moreau E 2007 *J. Phys. D: Appl. Phys.* **40.3** 605
[2] Benard N and Moreau E 2014 *Exp. in Fluids* **55.11** 1846.
[3] Kriegseis J, Simon B and Grundmann S 2016 *Appl. Mech. Rev.* **68** 020802-1
[4] Kotsonis M 2015 *Meas. Sci. Tech.* **26.9** 092001
[5] He C, Corke T C and Patel M P 2009 *J. Aircraft* **46.3** 864
[6] Kelley C, Bowles P, Cooney J, He C, Corke T, Osborne B, Silkey J and Zehnle J 2012 *50th AIAA Aerospace Sciences Meeting including the New Horizons Forum and Aerospace Exposition* p 906
[7] Joussot R, Hong D, Weber-Rozenbaum R and Leroy-Chesneau A 2010 *5th Flow Control Conference* p 4708
[8] Benard N, Braud P, Jolibois J and Moreau E 2008 *4th Flow Control Conference* p 4202
[9] Benard N, Jolibois J and Moreau E 2009 *J. Electrostat.* **67.2-3** 133
[10] Kelley C, Bowles P, Cooney J, He C, Corke T, Osborne B, Silkey J and Zehnle J 2014 *AIAA J.* **52.9** 1871
[11] Corke T, Mertz B and Patel M 2006 *44th AIAA Aerospace Sciences Meeting and Exhibit* p 1208
[12] Thomas F, Corke T, Iqbal M, Kozlov A and Schatzman D 2009 *AIAA J.* **47.9** 2169
[13] Forte M, Jolibois J, Pons J, Moreau E, Touchard G and Cazalens M 2007 *Exp. Fluids* **43.6** 917
[14] Belan M and Messanelli F 2015 *J. Electrostat.* **76** 278
[15] Messanelli F and Belan M 2017 *55th AIAA Aerospace Sciences Meeting, AIAA SciTech Forum (Grapevine, Texas)* AIAA 2017-0395 p 1
[16] Jukes T N and Choi K S 2013 *J. Fluid Mech.* **733** 370
[17] Wicks M, Thomas F, Corke T, Patel M and Cain A 2015 *AIAA J.* **53.11** 3404
[18] Kriegseis J, Grundmann S and Tropea C 2013 *New Results in Numerical and Experimental Fluid Mechanics VIII* (Berlin: Springer) p 209
[19] Messanelli F *Optimization of plasma actuators for flow control* 2017 (Phd Dissertation, Politecnico di Milano, Italy)
[20] Corke T, Enloe C and Wilkinson S 2010 *Annual Rev. Fluid Mech.* **42** 505